Xu et al. Fluids and Barriers of the CNS (2025) 22:22
https://doi.org/10.1186/s12987-025-00635-y

Fluids and Barriers of the CNS

RESEARCH Open Access

Hippocampal vascularization pattern and cerebral blood flow cooperatively modulate hippocampal tolerable amount of Aβ deposition in the occurrence of MCI

Yuhao Xu[1,2,3†], Hong Wei[2,4,6†], Rui Du[2], Ranchao Wang[2], Yan Zhu[2,5], Tian Zhao[2,5], Xiaolan Zhu[6,7*] and Yuefeng Li[1,2*]

Abstract

Background Aβ deposition in the brain does not necessarily lead to cognitive impairment, and that blood supply may have other unexplained regulatory effects on Aβ. Therefore, there appears to be a more complex relationship between blood supply, Aβ deposition, and cognitive impairment that warrants further exploration.

Methods This cohort study collected four longitudinal follow-up datasets, including a total of 281 subjects, followed for four years. Three-dimensional time-of-flight angiography and pseudo-continuous arterial spin labeling were used to assess hippocampal vascularization pattern (VP) and hippocampal cerebral blood flow (CBF). 11 C-Pittsburgh compound B (PiB)-PET/CT-based spatial measurements were used detect hippocampal PiB uptake as a reflection of hippocampal Aβ deposition. We explored the relationships between hippocampal blood supply (VP and CBF), hippocampal PiB uptake, and the occurrence of mild cognitive impairment (MCI) using a generalized nonlinear model.

Results We demonstrated the synergistic effect of hippocampal VP and CBF on predicting the occurrence of MCI. We conducted confirmation and quantification of the relationship between hippocampal blood supply and hippocampal PiB uptake. Additionally, the predicted value of PiB uptake based on hippocampal blood supply not only exhibited strong predictive efficacy for the occurrence of MCI (AUC = 0.831, $p < 0.001$), but was also validated in cerebral small vessel disease cohorts (AUC = 0.792, $p < 0.001$) and well validated in an independent cohort (Kappa = 0.741, $p < 0.001$).

Conclusions Overall, we reveal that hippocampal blood supply at baseline can regulate hippocampal PiB uptake, which reflects hippocampal tolerable amount of Aβ deposition and serves as an effective predictor for the occurrence of MCI, providing an important extension on the relationship between hippocampal blood supply and Aβ deposition.

Keywords Aβ deposition, Cerebral blood flow, Hippocampal vascularization pattern, Mild cognitive impairment

†Yuhao Xu and Hong Wei contributed equally to the work.

*Correspondence:
Xiaolan Zhu
zxl2517@163.com
Yuefeng Li
jiangdalyf@163.com

Full list of author information is available at the end of the article

Introduction

Cerebral blood supply serves as a crucial clue in unraveling the mechanisms of cognitive impairment [1, 2]. One major cause of cognitive impairment is thought to result from an imbalance between the deposition of the key molecule Aβ and the transport-clearance function carried out by cerebral blood supply [3–5]. Aβ deposition induces pathophysiological changes through multiple pathways, including synaptic dysfunction, neuroinflammation, and oxidative stress. These processes work synergistically, leading to neuronal dysfunction and cognitive decline [6, 7]. In this context, cerebral blood flow (CBF) plays several roles in clearing Aβ, such as facilitating the exchange between cerebrospinal fluid and interstitial fluid, maintaining the integrity of the blood-brain barrier, and promoting clearance through the brain's lymphatic system [8–12]. According to these traditional theories, it can be concluded that CBF primarily contributes to Aβ clearance, and an adequate blood supply may reduce Aβ deposition. However, recent studies have shown that both good CBF and significant Aβ deposition can coexist in the brains of healthy subjects [13, 14], which seems to deviate from the notion that CBF helps clear Aβ. Furthermore, the amount of Aβ deposition has been found to be positively correlated with CBF in cognition-related brain regions, such as the hippocampus, amygdala, and caudate nucleus [13–15]. These intriguing findings not only suggest that Aβ deposition does not necessarily lead to cognitive impairment, but also indicate that good CBF may play an additional regulatory role in this process. Therefore, further research is needed to better understand the complex relationship between blood supply, Aβ deposition, and cognitive impairment.

As the core brain area responsible for cognitive function, the hippocampus is an ideal target for observing the relationship between blood supply and Aβ deposition [16, 17]. However, unlike Aβ deposition, which can be accurately obtained in vivo [18, 19], current strategies for assessing blood supply to the hippocampal region require improvement. Recent studies have proposed the concept of hippocampal vascularization pattern (VP) and suggested the advantage of a mixed hippocampal VP (blood supply derived from the collateral branches of the posterior cerebral artery and the anterior choroidal artery) over a single VP (blood supply derived only from the collateral branches of the posterior cerebral artery) in protecting against cognitive impairment [20–22]. Therefore, for a more accurate assessment of hippocampal blood supply, both hippocampal VP and hippocampal CBF should be considered together. This is especially important because different combinations of distinct hippocampal VP and CBF may have additional protective or detrimental effects. Additionally, cerebral small vessel disease (CSVD) is a group of diseases that affect the structure and function of small blood vessels in the brain, characterized by reduced CBF and closely associated with cognitive impairment [23, 24]. Studies have shown that CSVD often coexists with Aβ pathology [12, 25]. In the hippocampus, it has been reported that CSVD can independently, or through Aβ-related pathways contribute to hippocampal degeneration in the early stages of cognitive impairment [25]. Therefore, the relationship between hippocampal VP, CBF, and Aβ deposition in CSVD also needs to be further evaluated.

In this study, we hypothesized that the hippocampal blood supply, composed of the hippocampal VP and CBF, may provide a tolerable amount of Aβ deposition in the hippocampus, and Aβ deposition exceeding the tolerable amount may lead to the occurrence of MCI. We used three-dimensional time-of-flight angiography (3D TOF) and pseudo-continuous arterial spin labeling (pCASL) to assess the hippocampal VP and hippocampal CBF. We also employed 11 C-Pittsburgh compound B (PiB)-PET/CT-based spatial measurements to detect hippocampal PiB uptake as a reflection of Aβ deposition. Our aim was to establish the cause-and-effect relationship among hippocampal blood supply, hippocampal Aβ deposition, and the occurrence of MCI, thereby providing a significant supplement to the theory of brain blood supply and the pathogenesis of cognitive impairment.

Methods

Subjects

Subjects were recruited through the Cognitive Disorders Research Center of Jiangsu University Hospital from January 2019 to June 2020. Two types of subjects, cognitively normal and MCI, were recruited. Cognitively normal subjects were recruited according to the following inclusion criteria: (1) age > 65 years; (2) normal cognitive function tests. Exclusion criteria: (1) history of acute cerebral infarction, cerebral hemorrhage, intracranial venous thrombosis, or epilepsy; (2) contraindications to PET-CT and MR; (3) presence of tumors or other serious systemic diseases; (4) alcohol or drug dependency, or regular coffee drinking (> 3 times per week); and (5) inability to cooperate with follow-up and examination. MCI Patients were recruited according to the following inclusion criteria: (1) age > 65 years; (2) meeting the diagnostic criteria for MCI as defined by Petersen et al. [26, 27]. These patients were also subjected to the same exclusion criteria above. A detailed medical history of each subject was recorded, and all subjects underwent a neurological examination and neuropsychological tests. A total of 222 subjects including 167 cognitively normal individuals and 55 MCI patients. Imaging assessments, including imaging assessment of CSVD, hippocampal VP, hippocampal CBF and hippocampal volume, were performed at baseline for all enrolled subjects. Based

on the CSVD assessment, the 167 cognitively normal subjects were divided into two groups consisting of 106 subjects without CSVD (CN group) and 61 subjects with CSVD (CSVD-CN group). Over a follow-up period of 4 years, cognitive changes were observed in three groups: the CN group, CSVD-CN group, and MCI group. Cognitive function assessments were conducted every three months. Subjects who developed MCI in the CN group, subjects who developed MCI in the CSVD-CN group, and subjects who developed Alzheimer's disease (AD) in the MCI group all underwent PiB-PET/CT examinations.

During the follow-up period, 8 subjects were excluded from the CN group (4 were lost to follow-up, 1 had a stroke, 1 was diagnosed with a tumor, and 2 were lost for other reasons); finally, 98 subjects were included in the analysis (Set 1), of whom 22 were diagnosed with MCI (MCI group) and 76 were not (non-MCI group). Four subjects were excluded from the CSVD-CN group (1 was lost to follow-up, 2 had a stroke, and 1 was lost for other reasons); finally, 57 subjects were included in the analysis (Set 2), of whom 18 were diagnosed with MCI (CSVD-MCI group) and 39 were not (CSVD-non-MCI group). Thirteen subjects were excluded from the MCI group (5 had other types of dementia but did not meet the criteria for AD diagnosis, 2 were lost to follow-up, 3 had a stroke, and 3 were lost for other reasons); finally, 42 subjects were included in the analysis (Set 3), of whom 16 were diagnosed with AD (AD group) and 26 were not (non-dementia group).

The same recruitment criteria were used to collect an independent validation cohort from the Fourth Affiliated Hospital of Jiangsu University. A total of 92 cognitively normal subjects were recruited. Baseline imaging data, including CSVD characteristics, hippocampal VP, and hippocampal CBF, were collected. The same follow-up procedures were performed for 4 years to observe cognitive changes. A total of 8 subjects were excluded during the follow-up period (2 were lost to follow-up, 1 had a stroke, 2 were diagnosed with a tumor, and 3 were lost for other reasons); finally, 84 subjects were included in the analysis (Set 4).

The study protocol flowchart is shown in Fig. S1.

Ethics statement

All participants provided written informed consent according to the Declaration of Helsinki and were reimbursed for travel expenses, and the study was approved by the Ethics Committee of the Affiliated Hospital of Jiangsu University and Fourth Affiliated Hospital of Jiangsu University (Ethics number: SWXYLL2019017).

Assessment of cognitive function

Assessment of cognitive function was performed by the respective assessment teams (nurses, psychologists, neuropsychologists and neurologists) of the two centers with reference to uniform criteria. Cognitive assessments were performed every three months. MCI was diagnosed with reference to MCI diagnostic criteria as defined by Petersen et al. [26, 27] and AD was diagnosed according to the NINCDS/ADRDA criteria [28].

Assessment of CSVD

To diagnose or exclude CSVD, all participants underwent MRI scans using a 3.0 T MRI system (Verio; Siemens, Erlangen, Germany) with a 32-channel head coil. The acquisition sequences included T1-weighted imaging, T2-weighted imaging, T2-fluid-attenuated inversion recovery, and susceptibility-weighted imaging. The images were reviewed by an experienced neuroimaging physician in a blinded fashion. Neuroimaging markers of CSVD include hemorrhagic (cerebral microbleed (CMB), cortical superficial siderosis) and nonhemorrhagic markers (white matter hyperintensities (WMH), lacunes, perivascular spaces) [29, 30]. Caps or pencil-thin lining periventricular WMH and/or punctate foci of deep WMH, which are both scored as grade 1 (mild) on the WMH Fazekas visual rating scale, are a common finding in aging and did not impact inclusion in the CN group [31]. CSVD was assessed comprehensively using total burden scores by calculating the presence of each of the 4 MRI features of CSVD [32, 33], including confluent deep WMH (Fazekas score 2 or 3) or irregular periventricular WMH extending into the deep white matter (Fazekas score 3), ≥ 1 lacune (< 15 mm), ≥ 1 CMB (< 5 mm) and moderate to severe basal ganglia EPVS. Each occurrence added 1 point to the total score, with total scores ranging from 0 to 4. A higher score indicated a more severe condition.

Assessment of hippocampal VP

3D TOF angiography was used to identify hippocampal VP. The TOF parameters were as follows: FOV = 240 mm × 212 mm, matrix size = 256 × 256, layer thickness = 0.3 mm, TR = 24 ms, and TE = 3.29 ms. Automatic segmentation of whole-brain T1 images using FSL FIRST was performed to generate structural masks of the whole hippocampus (left/right) [34]. In addition, structural hippocampus masks were manually checked and corrected if necessary using FSLVIEW. The corrected T1 hippocampus masks were coregistered to TOF images using ANT coregistration algorithms [35]. To analyze the relationship between arteries and brain structures, TOF MRA data were superimposed on the T1 images and viewed in coronal, sagittal and transverse orientations. According to the classification criteria of hippocampal VP proposed by Perosa et al. [20], each hippocampus was classified into one of two categories as shown in Fig. 1A.: a hippocampus with a single supply (a single supply by the

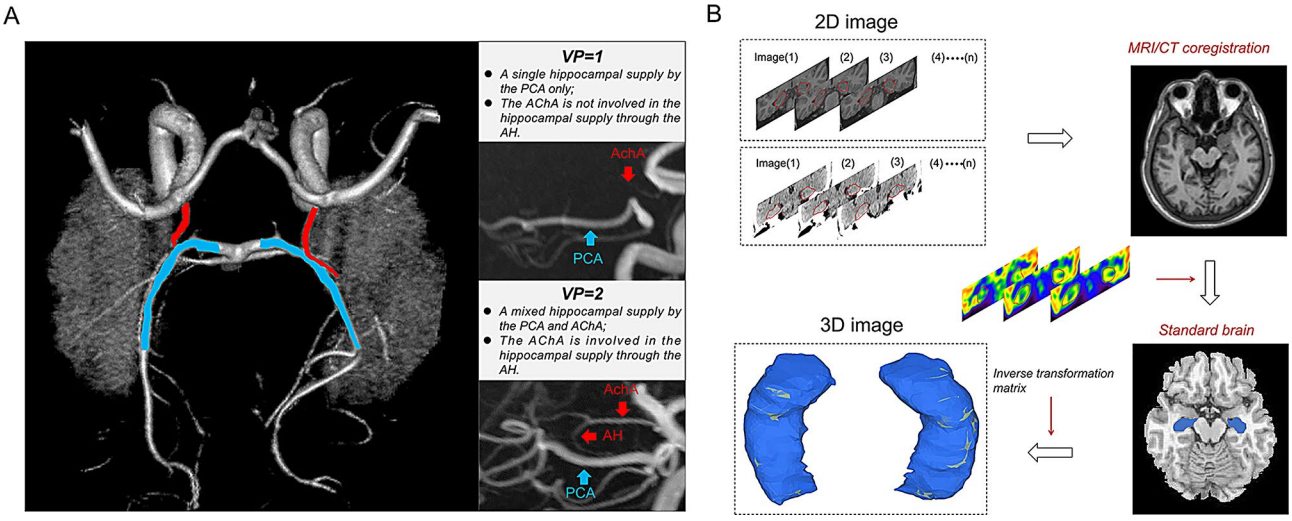

Fig. 1 Assessment of hippocampal VP and Aβ uptake. **A** A 3D TOF MRA reconstruction with the hippocampal mask. On the left: main vessels involved in the hippocampal blood supply. Blue indicates the posterior cerebral artery (PCA), and red indicates the anterior choroidal artery (AChA). On the top right: A single hippocampal supply by the PCA only; the AChA is not involved in the hippocampal blood through the anterior hippocampal artery (AH). On the bottom right: A mixed hippocampal supply by the PCA and AChA; the AChA is involved in hippocampal supply through the AH. **B** 3D imaging of hippocampal PiB uptake. Registering the CT image to the MRI. Integrating the PET image into the resulting MRI/CT fused imaging space to generate PET/CT and MRI registration. Normalizing the registered images to the Montreal Neurological Institute (MNI) space and applying smoothing. Extracting and calculating the PiB uptake of the entire hippocampal region, followed by reconstruction and spatial visual assessment of Aβ quantification on a 3D view

posterior cerebral artery) or a hippocampus with a mixed supply (a mixed supply from both the posterior cerebral artery and the anterior choroidal artery). Bilateral hippocampal VP was assessed separately with a score of 1 or 2 on each side. Hippocampal VP = left hippocampal VP + right hippocampal VP.

Hippocampal CBF

The resting CBF of all subjects was collected at baseline for observation. The hippocampal CBF maps were acquired using a pCASL sequence with a three-dimensional gradient and spin echo readout [36]. The following parameters were used: pulse duration = 1.5 s, one of four post-labeling delays (PLDs) = 1.5, 2, 2.5, or 3 s, no blood flow gradient, GRAPPA-2, repetition time = 3.5/3.9/4.4/4.9 s, echo time = 22 ms, and voxel size = 3.4 × 3.4 × 5.0. For M0 images the following parameters were used: repetition time = 6 s, PLD = 4 s, and acquisition time = 12 s. For each PLD, 12 pairs of marker images and control images were collected, and the total collection time was 6 min. pCASL images were postprocessed and analyzed in MATLAB 2010a (MathWorks, Natick. MA) and SPM12 software. The pCASL time series were motion corrected, pairwise subtracted, and time-averaged to acquire the ΔM(i) image. pCASL images were registered with T1 structural images, and the hippocampus was selected as the region of interest (ROI) to quantify CBF. CBF was calculated as follows:

$$f(i)=\frac{\lambda\cdot\Delta M\cdot R_{1a}}{2\cdot\alpha\cdot M0\left[\exp\left(\left(\min\left(\delta-\omega(i),0\right)-\delta\right)R_{1a}\right)-\exp\left(-\left(\tau-\omega(i)\right)R_{1a}\right)\right]}\left[ml/g/s\right]$$

where R1a is the longitudinal relaxation rate of blood, M0 is the equilibrium magnetization intensity of brain tissue, α is the labeling efficiency (0.8), τ is the duration of the labeling pulse (1.5 s), and λ is the tissue-blood partition coefficient (0.9 g/mL). The final CBF was calculated as the mean of the estimated CBF for each PLD. Hippocampal CBF = left hippocampal CBF + right hippocampal CBF.

Hippocampal volume measurement

Hippocampal volume measurements were performed using high-resolution structural MRI with a three-dimensional magnetization-prepared fast gradient echo sequence with the following parameters: 192-layer sagittal slices, TR = 2530 ms, TE = 2.26 ms, flip angle = 90°, voxel size = 1 mm×1 mm×1 mm, display field = 256 mm×256 mm, matrix size = 256 × 256, layer thickness = 1 mm, layer gap = 0 mm, and scan time = 10 min, 8 s. The volume was calculated using FreeSurfer (http://surfer.nmr.mgh.harvard.edu/) as described [37, 38]. This processing step included motion correction, removal of noncerebral tissue from the image using a hybrid watershed/surface deformation procedure, automatic talairach transformation, intensity normalization, determination of gray matter/white matter boundaries, automatic topology correction, and surface deformation after calculation of intensity gradients to optimally place gray/white and gray/cerebrospinal fluid boundaries at locations with the greatest intensity change, ultimately

defining transitions to other tissue categories. Quality control was performed by visual inspection as described in a recent protocol (http://enigma.loni.ucla.edu/protocols/) and checked for outliers. Hippocampal volume = left hippocampal volume + right hippocampal volume.

Assessment of hippocampal Aβ deposition by 11 C-PiB-PET/CT

11 C-PiB-PET/CT-based spatial measurements were used detect hippocampal PiB uptake as a reflection of hippocampal Aβ deposition. Subjects were seated quietly for 30 min and then imaged using a PET/CT scanner (Discovery ST4, GE Healthcare, Chicago, IL, United States) in 3D mode for 11 C-PiB-PET/CT [39, 40]. 11 C-PiB was injected intravenously according to the subject's body weight (mean: 617 MBq; range: 413–697 MBq), and PIB PET images were acquired starting after an approximately 50-minute uptake period. Attenuation correction and anatomical localization were performed using a low-dose CT scan without contrast enhancement. The axes of the two systems were mechanically aligned for optimal coincidence. After 20 min of CT data acquisition, PET data acquisition was started in 3D mode, consisting of four 5-minute dynamic frames. If motion was detected, the individual frames of the PiB dynamic sequence were realigned, and then an average image was created [41]. Afterwards, utilize MATLAB software to process the images, registering the CT image to the MRI. Subsequently, integrate the PET image into the resulting MRI/CT fused imaging space to generate PET/CT and MRI registration. Normalize the registered images to the Montreal Neurological Institute (MNI) space and apply smoothing. Finally, extract and calculate the PiB uptake of the entire hippocampal region using the MarsBaR toolbox, reconstruct, and conduct spatial visual assessment of Aβ quantification on a 3D view (Fig. 1B). The axial and face forward MRI, CT, and PiB-PET images of representative individuals were shown in Fig. S2. PiB uptake was evaluated separately for each hippocampus. Hippocampal PiB uptake = left hippocampal PiB uptake + right hippocampal PiB uptake.

Statistical analysis

Data analysis was performed using SPSS 23.0 (SPSS, Inc.) and GraphPad Prism 8.0. The normality of data distribution was analyzed by the Shapiro-Wilk test. Continuous variables that conform to the normal distribution are expressed as mean ± standard deviation, and standard deviation is used as the error bar. Continuous variables that do not conform to the normal distribution are expressed as the median (minimum value, maximum value), and categorical variables are expressed as percentages. Between-group differences in variables were evaluated using one-way ANOVA, Mann-Whitney test, or Chi-square tests, with analysis of covariance employed to adjust for covariate effects on observed variables. Pearson or Spearman correlation analysis was used to analyze the correlation between variables. Logistic regression forward selection with 10-fold cross-validation was utilized to evaluate the predictive model of hippocampal VP and CBF on the occurrence of MCI, and the ROC curve was drawn. The least squares method was used to construct a nonlinear regression model based on baseline hippocampal VP and hippocampal CBF to predict the hippocampal PiB uptake, and the leave-one-out method was used for cross-validation. The Bland-Altman method was used to evaluate the consistency between the predicted value and the actual value of hippocampal PiB uptake. The Kappa coefficient was used to evaluate the agreement between the predicted and actual outcomes. All analyses were two-tailed, and $p < 0.05$ was considered to indicate a statistically significant difference.

Results

Demographic data

A total of four datasets, labeled from Set 1 to Set 4, were utilized in this study. The flowchart illustrating the use of each dataset is shown in Fig. 2. Set 1 was used to achieve the following objectives: (1) To observe the relationship between hippocampal blood supply (VP and CBF) and the occurrence of MCI. (2) To analyze the relationship between hippocampal blood supply and hippocampal PiB uptake, and construct a nonlinear regression model predicting hippocampal PiB uptake. (3) To test the predictive efficacy of the predicted value of hippocampal PiB uptake for the occurrence of MCI. Set 2 was used to evaluate the predictive efficacy of the predicted value of hippocampal PiB uptake for the occurrence of MCI in the CSVD-CN group. Set 3 was used to assess whether the predicted value of hippocampal PiB uptake could predict the conversion of MCI to AD. Set 4 served as an external independent validation to confirm the predictive efficacy of the predicted value for MCI. The demographic information of subjects at baseline in each dataset is shown in Table S1. The prevalences of transitioning from CN to MCI in Set 1, from CSVD-CN to CSVD-MCI in Set 2, and from MCI to AD in Set 3 were 22.45%, 31.57%, and 38.09%, respectively, which were consistent with extant reports [42–44].

The synergistic effect of baseline hippocampal VP and CBF on the occurrence of MCI

In Set 1, both the baseline hippocampal VP and CBF in the MCI group lower than those in the non-MCI group, even after adjusting for confounding factors ($p < 0.05$) (Fig. 3A-B). Additionally, a significant synergistic phenomenon was observed that individuals with high hippocampal VP and high CBF had the lowest incidence

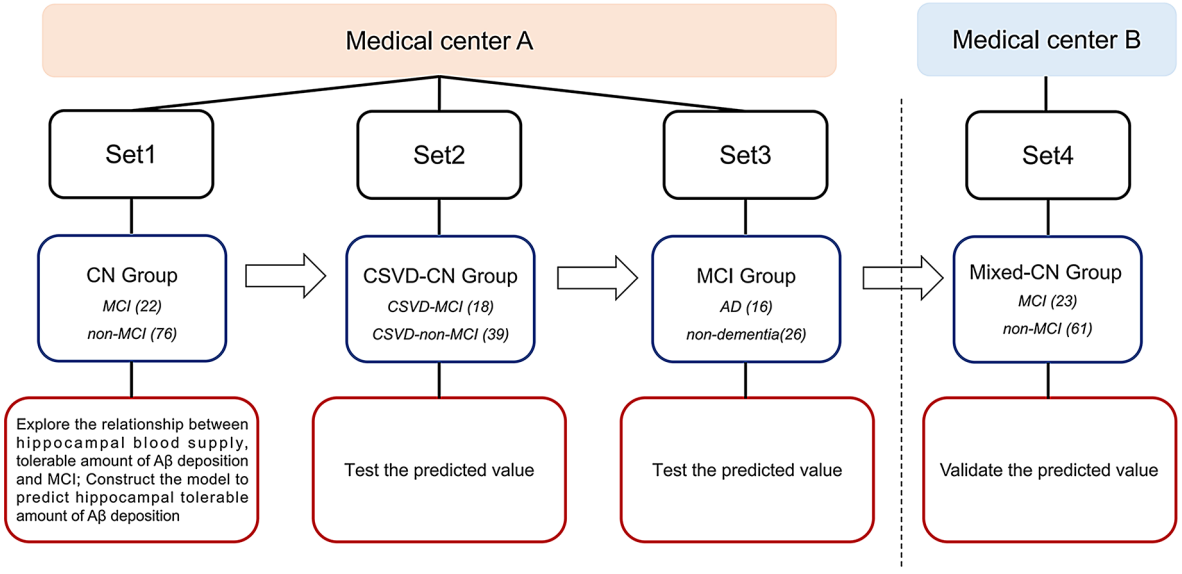

Fig. 2 Flow chart showing the use of each dataset

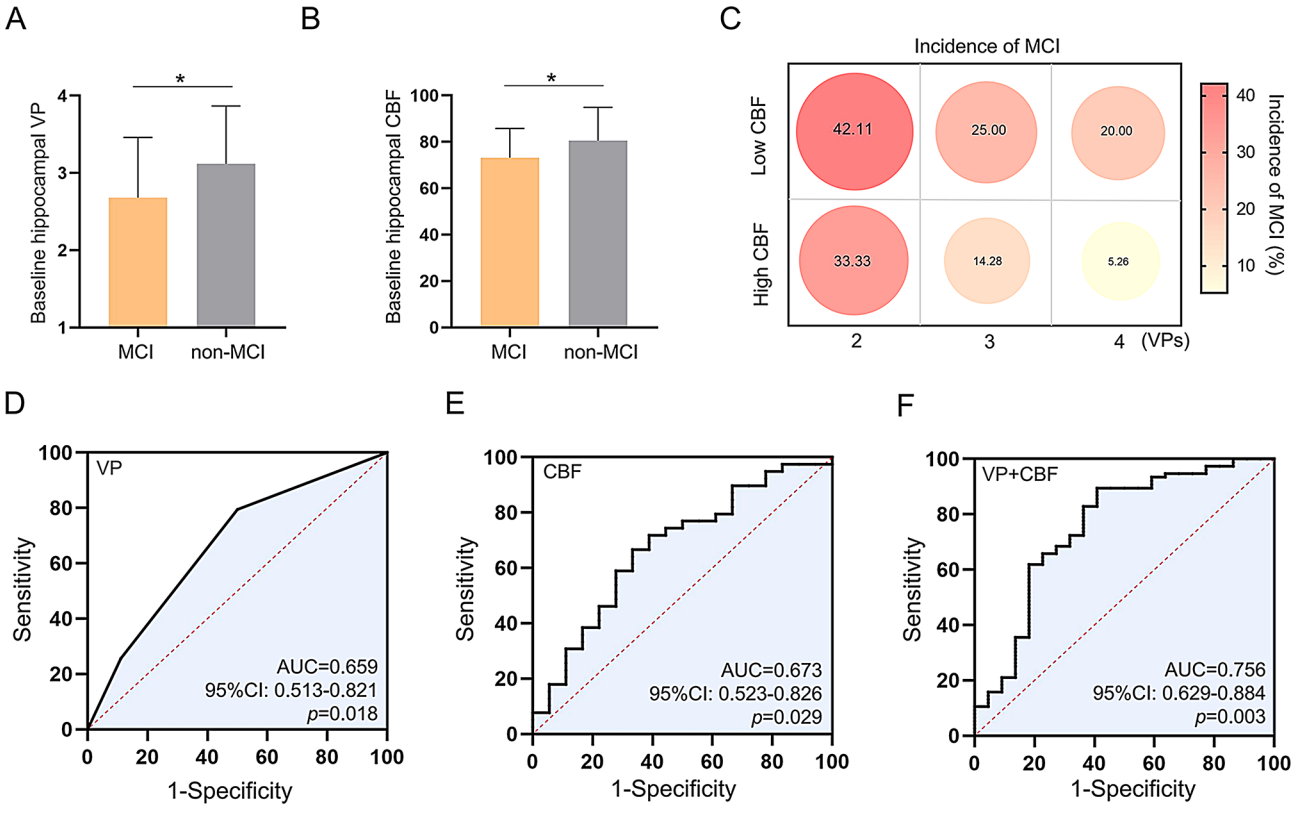

Fig. 3 The relationship between baseline hippocampal blood supply and MCI occurrence. **A-B** Baseline hippocampal VP and baseline hippocampal CBF were lower in the MCI group compared to the non-MCI group. **C** Incidence of MCI under different combinations of baseline hippocampal VP and baseline hippocampal CBF (the median hippocampal CBF was used as a cut-off value to determine high and low CBF; the color scale reflects the incidence of MCI (%)). **D-F** ROC curves of baseline hippocampal VP, baseline hippocampal CBF, and the combination of both to predict MCI occurrence. *$p < 0.05$, **$p < 0.01$

of MCI (Fig. 3C). Further analysis confirmed that baseline hippocampal VP (*OR*: 0.913; 95% *CI*: 0.853 ~ 0.970; $p < 0.001$) and CBF (*OR*: 0.935; 95% *CI*: 0.903–0.967; $p < 0.001$) were independent protective factors for the occurrence of MCI. Moreover, the synergistic effect and predictive efficacy between the two (VP + CBF) were also confirmed (*OR*: 0.873; 95% *CI*: 0.808 ~ 0.937; $p < 0.001$) (ROC: AUC_{VP}=0.659, $p < 0.05$; AUC_{CBF}=0.673, $p < 0.05$; $AUC_{(VP+CBF)} = 0.756$, $p < 0.01$) (Fig. 3D-F).

The relationship between baseline hippocampal blood supply (VP and CBF) and hippocampal PiB uptake

Among MCI patients in Set 1, hippocampal PiB uptake exhibited significant individual differences, ranging from a maximum of 6.32 to a minimum of 11.49 (Fig. 4A). This variability was significantly associated with hippocampal blood supply at baseline; MCI patients with high hippocampal PiB uptake tended to have high VP and CBF at baseline, while those with low hippocampal PiB uptake tended to have low VP and CBF at baseline ($p < 0.01$) (Fig. 4B-D). This strongly suggests that the

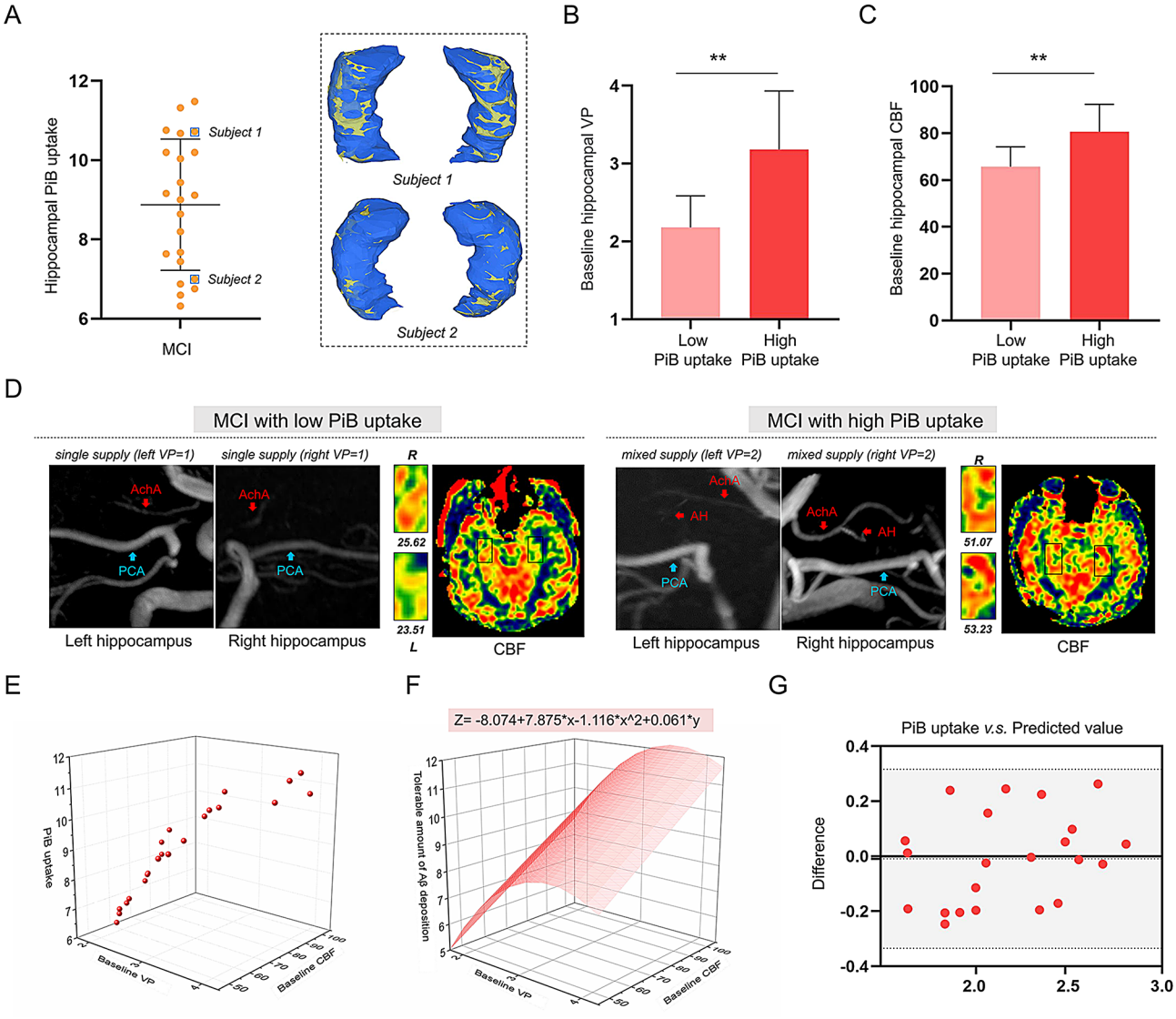

Fig. 4 The relationship between baseline hippocampal blood supply and hippocampal PiB uptake. **A** Left panel: hippocampal PiB uptake at the MCI stage exhibit large individual differences (max 11.49, min 6.32). Right panel: representative 3D reconstructed images of PiB uptake in individual hippocampus. **B-C** Baseline hippocampal VP and baseline hippocampal CBF were lower in MCI patients with low hippocampal PiB uptake than in MCI patients with high hippocampal PiB uptake (the median hippocampal PiB uptake was used as a cut off value to determine high and low). **D** Representative individual images of hippocampal VP and corresponding hippocampal CBF in MCI patients with low hippocampal PiB uptake and high hippocampal PiB uptake. **E** The three-dimensional scatter plot of hippocampal PiB uptake (tolerable amount of Aβ deposition) versus baseline hippocampal VP and baseline hippocampal CBF. **F** The nonlinear model predicting the hippocampal PiB uptake based on baseline hippocampal VP and baseline hippocampal CBF. **G** Bland–Altman plots showed good agreement between PiB uptake and the predicted value. *$p < 0.05$, **$p < 0.01$

hippocampal VP and CBF at baseline may determine the hippocampal PiB uptake (Aβ deposition), which contributes to the development of MCI. Subsequently, we used hippocampal PiB uptake at the onset of MCI as the threshold for hippocampal tolerable amount of Aβ deposition. The nonlinear least squares method was used to construct an equation for predicting the hippocampal PiB uptake (the tolerable amount of Aβ deposition) based on hippocampal VP and hippocampal CBF. Additionally, the leave-one-out method was employed for cross-validation to obtain a nonlinear model that effectively predicts the hippocampal PiB uptake. (Z=-8.074 + 7.875*x-1.116*x^2 + 0.061*y; Z is the predicted value of hippocampal PiB uptake; X is the value of baseline hippocampal VP; Y is the value of baseline hippocampal CBF) (Fig. 4E-G).

The predicted value of hippocampal PiB uptake based on hippocampal blood supply can predict the occurrence of MCI

We analyzed the predictive efficacy of the predicted value of hippocampal PiB uptake for the occurrence of MCI. In Set 1, we calculated the corresponding predicted values based on the baseline hippocampal VP and CBF of 98 subjects, which represent each individual's tolerable amount of Aβ deposition (Fig. S3A). Further results showed that the predicted values were significantly lower in the MCI group compared to the non-MCI group and exhibited outstanding predictive efficacy for MCI occurrence (AUC = 0.831; $p < 0.001$) (Fig. 5A-B). Notably, the predicted values in MCI patients were not correlated with baseline hippocampal volume ($p > 0.05$) but were associated with the patient's age, history of hypertension, and diabetes ($p < 0.001$) (Table S2). In addition, patients with CSVD (Set 2), representing a sample of reduced CBF, were used to assess the predictive efficacy of the predicted values for MCI occurrence. As expected, CSVD-CN group in set 2 showed disadvantaged baseline hippocampal VP and CBF, along with a higher incidence of MCI compared to the CN group in set 1 ($p < 0.05$) (Fig. S4). After a four-year follow-up of CSVD-CN patients, we observed significant individual differences in hippocampal PiB uptake within the CSVD-MCI group (PiB uptake ranging from a minimum of 5.94 to a maximum of 10.17) (Fig. 5C). Afterward, we calculated the corresponding predicted values based on the baseline hippocampal VP and CBF of 57 subjects in set 2 (Fig. S3B). Interestingly, although the predicted value still differed between CSDV-MCI group and CSDV-non-MCI group, the predictive efficacy of the predicted values for the occurrence of MCI in set2 is significantly lower compared to that in set 1, (ROC: 0.688 vs. 0.831) (Fig. 5D-E). Additionally,

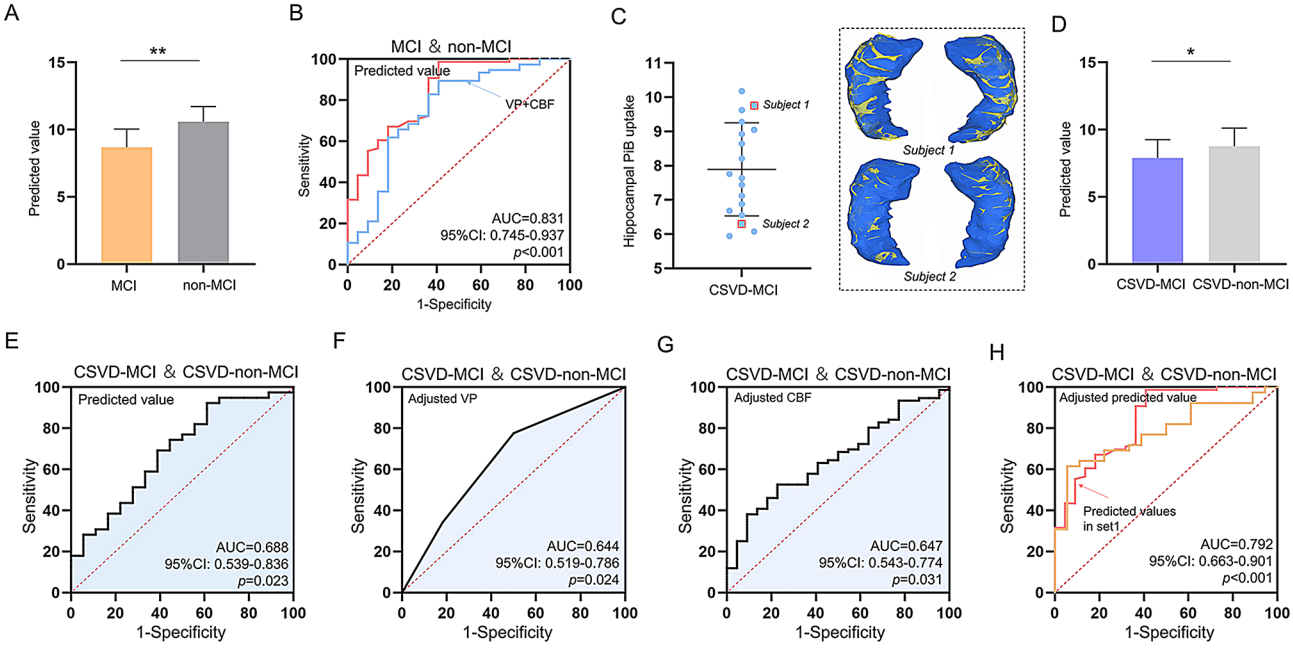

Fig. 5 The relationship between the predicted value and the occurrence of MCI. **A-B** The predicted values were lower in the MCI group compared to the non-MCI group and exhibited outstanding predictive efficacy for MCI occurrence. **C** Left panel: hippocampal PiB uptake of the CSVD-MCI group at MCI stage exhibit large individual differences (max 10.17, min 5.94). Right panel: Representative 3D reconstructed images of PiB uptake in the hippocampi of CSVD-MCI subjects. **D-E** The predicted values were lower in the CSVD-MCI group compared to the CSVD-non-MCI group but exhibited not good predictive efficacy for MCI occurrence. **F-G** Baseline hippocampal VP and CBF demonstrated predictive efficacy for the occurrence of MCI in the CSVD-CN group after correcting for CSVD scores. **H** The predictive efficacy of predicted values in the CSVD-CN group approaching the predictive efficacy of predicted values observed in the CN group after correcting for CSVD scores. *$p < 0.05$, **$p < 0.01$

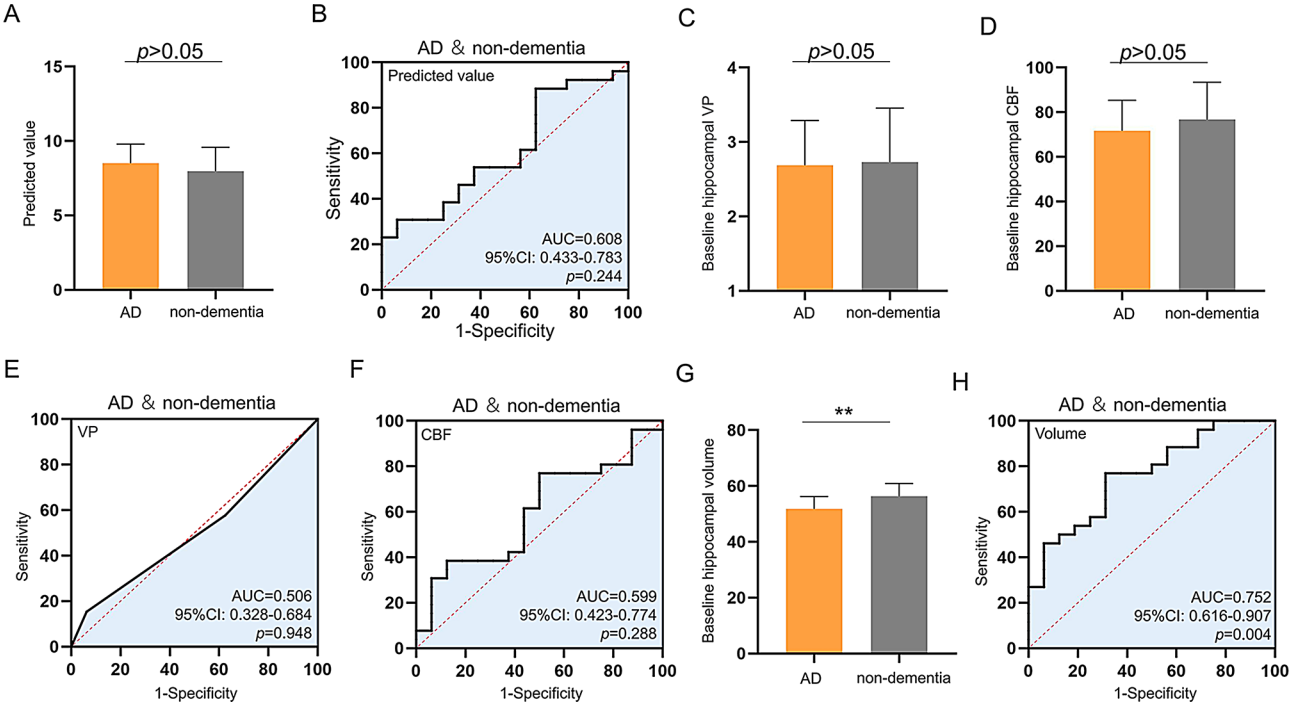

Fig. 6 The relationship between the predicted value and the occurrence of AD in the MCI group. **A-B** The predicted value did not show significant differences between the AD group and the non-dementia group, nor could they predict the conversion of MCI to AD. **C-D** Baseline hippocampal VP and baseline hippocampal CBF showed no significant differences between the AD group and the non-dementia group. **E-F** Baseline hippocampal VP and baseline hippocampal CBF could not predict the transformation of MCI to AD. **G-H** Baseline hippocampal volume was lower in AD group than non-dementia group and showed predictive power for MCI to AD conversion. *$p < 0.05$, **$p < 0.01$

there were no differences in baseline VP, CBF, and CSVD scores between the CSVD-MCI and CSVD-non-MCI groups in set 2, and these baseline measures did not have predictive efficacy for the occurrence of MCI ($p > 0.05$) (Fig. S5). However, after correcting for CSVD scores as a covariate, baseline hippocampal VP and CBF demonstrated predictive efficacy for the occurrence of MCI in the CSVD-CN group (Fig. 5F-G). The predictive efficacy of the predicted values significantly increased, approaching that observed in set 1 (Fig. 5H).

The predicted value of hippocampal PiB uptake is not useful in predicting the conversion from MCI to AD

We further investigated whether the predicted value could predict the conversion from MCI to AD. In Set 3, we calculated the corresponding predicted values based on the baseline hippocampal VP and CBF of 42 subjects (Fig. S3C). However, the predicted values did not show significant differences between the AD group and the non-dementia group, nor did they predict the conversion of MCI to AD, even after adjusting for cofactors ($p > 0.05$) (Fig. 6A-B). When comparing hippocampal blood supply, we found that, after adjusting for cofactors, neither baseline hippocampal VP nor CBF differed significantly between the AD group and the non-dementia group ($p > 0.05$) (Fig. 6C-D). Furthermore, baseline hippocampal VP and CBF could not predict the transformation of MCI to AD ($p > 0.05$) (Fig. 6E-F). Additionally, no correlation was observed between baseline hippocampal blood supply and hippocampal PiB uptake in AD patients ($p > 0.05$) (Fig. S6). The predictive power for MCI to AD conversion was only evident in baseline hippocampal volume at MCI stage ($p < 0.01$) (Fig. 6G-H).

Validation

In the independent validation set (Set 4), among 84 cognitively normal individuals followed for 4 years, the incidence of MCI was 27.38%, consisting of 23 cases of MCI and 61 cases of non-MCI. The sensitivity of the predicted values in predicting the occurrence of MCI was 0.869 (20/23), the specificity was 0.901 (55/61), and the accuracy was 89.29%, which was in good agreement with the actual outcome (Kappa = 0.741, $p < 0.001$). However, there were nine subjects whose predicted outcomes did not match the actual outcomes, including six false positives and three false negatives. The majority of false positives had a total hippocampal VP of 3 combined with low hippocampal CBF (4/6), while the false negatives typically had a total hippocampal VP of 3 combined with high hippocampal CBF (3/3).

Discussion

In this longitudinal follow-up study involving multiple sample sets, we used hippocampal VP and CBF as comprehensive indicators to assess hippocampal blood supply, while hippocampal PiB uptake served as a marker for Aβ deposition. We considered hippocampal PiB uptake detected at the onset of MCI to represent the hippocampal tolerable amount of Aβ deposition. For the first time, we elucidated the relationship between baseline hippocampal blood supply, the tolerable amount of hippocampal Aβ deposition, and the occurrence of MCI. Our findings suggest that hippocampal VP and CBF influence the occurrence of MCI by affecting the hippocampal tolerable amount of Aβ deposition (as reflected by hippocampal PiB uptake). Consequently, we constructed a model to predict the hippocampal tolerable amount of Aβ deposition, and the predicted values effectively forecasted the occurrence of MCI. These positive results were not only corroborated in CSVD subjects but also reproduced in an independent validation set.

Despite numerous studies focusing on hippocampal blood supply and MCI [20, 45, 46], the crucial question of whether there are differences in the risk of MCI between individuals with different combinations of hippocampal VP and hippocampal CBF seems to have been left unstudied. More specifically, hippocampal VP and hippocampal CBF have not been considered together as factors in previous studies. This scientific question is particularly important because the hippocampal vascular structure is different from that of most brain nuclei, with hippocampal VP have distinctly diverse layouts [22, 45, 47]. Our results not only confirm that hippocampal VP and hippocampal CBF are independent factors influencing the occurrence of MCI but also demonstrate their combined effect. Here, we explain the differential cognitive outcomes in individuals with the same hippocampal VP or the same level of hippocampal CBF, Presenting the view that individuals with higher hippocampal CBF have a lower risk of MCI at an equal hippocampal VP, while individuals with higher hippocampal VP tend to have better cognitive outcomes at an equal level of hippocampal CBF. In other words, individuals with low hippocampal VP and low hippocampal CBF are at high risk of MCI, while individuals with high hippocampal VP and high hippocampal CBF are most likely to be immune to MCI.

Aβ deposition in the brain is considered the hallmark neuropathological alteration occurring in MCI and AD, and it is more pronounced in specific, vulnerable brain regions, notably the hippocampus [48–50]. In the transition from quantitative to qualitative Aβ deposition leading to cognitive impairment, different individuals exhibit significant differences in their tolerable amount of Aβ deposition. This concept is supported by evidence of high loads of Aβ deposition in cognitively normal populations [13, 14]. In this study, we observed hippocampal Aβ deposition (PiB uptake) at the onset of MCI. The results from PiB-PET/CT showed significant within-group differences in hippocampal PiB uptake in the MCI group, which supports the view that there are individual differences in the hippocampal tolerable amount of Aβ deposition. Furthermore, MCI patients with high hippocampal Aβ deposition tended to have higher hippocampal VP and CBF at baseline, while patients with low Aβ deposition tended to have lower hippocampal VP and CBF at baseline. This observation underscores a potential correlation between hippocampal blood supply and the hippocampal tolerable amount of Aβ deposition, supporting our hypothesis that individuals vary in their hippocampal tolerable amount of Aβ deposition, and that hippocampal VP and CBF may jointly influence the occurrence of MCI by affecting the hippocampal tolerable amount of Aβ deposition.

To further observe the specific relationship between hippocampal blood supply and hippocampal tolerable amount of Aβ deposition, we used hippocampal PiB uptake at the onset of MCI in patients as the threshold for tolerable amount of Aβ deposition. Based on baseline hippocampal VP and hippocampal CBF, we fitted a nonlinear regression equation that can predict the hippocampal tolerable amount of Aβ deposition. The predicted value showed good predictive efficacy for the occurrence of MCI. Moreover, in the CSVD-CN group, after adjusting for the burden of CSVD, the predicted value continued to demonstrate strong predictive efficacy for the occurrence of MCI. This suggests that the predicted value has broad applicability for MCI arising from various disease states, and correcting for confounding factors may enhance prediction accuracy. Our study also revealed that, during follow-up of MCI patients in Set 3, baseline hippocampal VP and hippocampal CBF were unable to predict the conversion from MCI to AD. This finding implies a stage-dependent relationship between hippocampal VP, hippocampal CBF, and the hippocampal tolerable amount of Aβ deposition. We hypothesize that during the transition from normal cognition to MCI, Aβ deposition in the hippocampus is in a quantitative stage, with hippocampal blood supply playing a protective role. However, when Aβ deposition exceeds the tolerable amount supported by hippocampal blood supply, MCI develops. After MCI onset, the equilibrium between hippocampal blood supply and Aβ deposition is disrupted, making it harder to gauge disease progression. Additionally, in an independent validation set (Set 4), we confirmed that the predicted value of hippocampal tolerable amount of Aβ deposition exhibits good sensitivity, specificity, and accuracy in predicting the occurrence of MCI. Moreover, false positives and false negatives were predominantly in individuals with three parental vessels

supplying the bilateral hippocampus. This implies that individuals receiving bilateral hippocampal blood supply from the three primary vessels may manifest considerable variability in vascular reserve, which is an important factor to consider in clinical practice.

In terms of imaging technology, for feasibility and multicenter data standardization, we optimized the parameters of 3.0T TOF and achieved discrimination of the proximal blood vessel source of the hippocampal artery. While contrast-enhanced MR angiography can offer better vascular resolution, the use of contrast agents may impose additional physiological burdens on subjects, which was not considered in this study [51]. Blood oxygenation level-dependent (BOLD) MRI is another tool that assesses blood oxygen content and can also be used to evaluate blood supply reserve. However, BOLD-MRI only reflects the immediate state of the reserve and cannot assess long-term effects [52, 53]. In the assessment of CBF, activity-evoked CBF, while useful for reflecting how CBF is influenced by task states, requires better patient cooperation and tends to have lower stability in practice with greater individual variability. Due to these factors, it is not ideal for evaluating CBF in our study. Therefore, we chose resting CBF for our observations. To evaluate hippocampal CBF, we used the 3D-pCASL technique, which is less sensitive to magnetic sensitivity and motion artifacts due to its fast spin-echo sequence acquisition and spiral K-space filling [54]. Moreover, 3D pCASL offers advantages such as being economical, convenient, and non-radioactive compared to traditional perfusion imaging techniques. It also provides a higher signal-to-noise ratio and better reproducibility than other ASL techniques, including continuous ASL and pulsed ASL [55]. Most importantly, we used PiB-PET to visualize in vivo brain Aβ deposition and matched PiB-PET/CT images with MRI brain images to standardize the data as much as possible and optimize our analysis. Additionally, we performed three-dimensional reconstruction of the hippocampus and Aβ deposition, allowing for accurate assessment of hippocampal Aβ deposition in different individuals. This process provided assurance for the subsequent data analysis.

Different from retrospective studies, which previously represented the main approach, our study was a prospective cohort study with a follow up period of up to 4 years. This prospective design allows us to largely avoid selection bias and obtain a large amount of prospective data on confounding factors. Although our study involved multiple sample sets, the study flow was uniformly managed according to a standardized diagnostic and management protocol. We conducted complete clinical, cognitive, and imaging assessments at each time interval, ensuring data integrity and confirming key findings in an independent validation set. Additionally, previous studies have shown that caffeine can lead to transient acute decreases in CBF [56]. In our study, we excluded subjects who were frequent coffee drinkers and required participants to abstain from coffee intake for one week prior to MRI scanning. It is also worth noting that while we simultaneously observed both hippocampal VP and CBF in the study, which may pose certain challenges for clinical patient compliance, the stability of hippocampal VP suggests that, in future clinical work, repeat examinations of hippocampal VP may be avoided, improving follow-up efficiency and compliance. Furthermore, neuronal activity can increase CBF [57, 58]. This provides a new potential avenue for intervention: if methods can be developed to sustain the CBF increase induced by neuronal activity, it may enhance the hippocampus's tolerance to Aβ deposition, which could offer a promising direction for the prevention and treatment of MCI in the future.

Our study still has some limitations. Although we tried to correct for clinical confounding factors as much as possible, it is undeniable that there will be unconsidered confounding factors that were not excluded. Additionally, the effect of the ApoE gene on MCI and AD was not considered, and MCI subtype differentiation was not performed. The role of the venous system was not considered. Furthermore, the sample size was relatively small, and larger-scale studies are needed to further clarify and optimize the assessment of cerebral blood flow in relation to Aβ deposition and to validate our findings. It is worth noting that this study only measured hippocampal CBF and PiB uptake at a single time point and did not observe their changes over time during disease progression. Longitudinal studies on the dynamic changes of CBF and PiB uptake are crucial for a better understanding of hippocampal Aβ deposition patterns and the progression of disease characteristics, which requires further exploration.

Conclusion

In summary, we demonstrated that hippocampal VP and CBF synergistically determine hippocampal tolerable amount of Aβ deposition in the occurrence of MCI. we constructed a predictive model for the hippocampal tolerable amount of Aβ deposition based on hippocampal VP and CBF, which accurately forecasts the occurrence of MCI. Our study findings reveal that baseline hippocampal VP and CBF can influence the onset of MCI by regulating hippocampal tolerable amount of Aβ deposition, which provides a significant extension to the existing understanding of the relationship between blood supply and Aβ.

Abbreviations

AChA	Anterior choroidal artery
AD	Alzheimer's disease
AH	Anterior hippocampal artery

AUC	Area under the curve
BOLD	Blood oxygenation level-dependent
CBF	Cerebral blood flow
CI	Confidence interval
CMB	Cerebral microbleed
CN	Cognitively normal
CSVD	Cerebral small vessel disease
DM	Diabetes mellitus
HBP	High blood pressure
MCI	Mild cognitive impairment
OR	Odds ratio
PCA	Posterior cerebral artery
pCASL	Pseudo-continuous arterial spin labeling
PiB	11 C-Pittsburgh compound B
PLD	Post-labeling delay
ROC	Receiver operating characteristic
ROI	Region of interest
TOF	Three-dimensional time-of-flight
VP	Vascularization pattern
WMH	White matter hyperintensities

Supplementary Information

The online version contains supplementary material available at https://doi.org/10.1186/s12987-025-00635-y.

Supplementary Material 1

Acknowledgements
We sincerely appreciate the participants in our study.

Author contributions
Y.X. and H.W. extracted the study cohort, analyzed the data, and performed clinical follow-up and validation. Y.X. and R.D. contributed their clinical expertise. R.W., Y. Z. and T. Z. performed imaging data collection, analysis and follow-up. Y.X. and R.D wrote the paper, with revision advice provided by Y.L. and X.Z. All authors have read and approved the manuscript.

Funding
This work was supported by National Natural Science Foundation of China (82101431) and Jiangsu Provincial Key Research and Development Plan (BE2021693).

Data availability
The data supporting the findings from this study are available in the main manuscript and supplementary materials. Any other raw data or non-commercial material used in this study are available from the corresponding author upon request.

Declarations

Ethics approval and consent to participate
All participants provided written informed consent according to the Declaration of Helsinki and were reimbursed for travel expenses, and the study was approved by the Ethics Committee of the Affiliated Hospital of Jiangsu University and Fourth Affiliated Hospital of Jiangsu University (Ethics number: SWXYLL2019017).

Consent for publication
Not applicable.

Competing interests
The authors declare no competing interests.

Author details
[1]Department of Radiology, Affiliated People's Hospital of Jiangsu University, Zhenjiang 212001, China
[2]Department of Neuroimaging Laboratory, School of Medicine, Jiangsu University, Zhenjiang, Jiangsu 212013, China
[3]Department of Neurology, Affiliated Hospital of Jiangsu University, Zhenjiang 212001, China
[4]Department of Neurology, The Fourth Affiliated Hospital of Jiangsu University, Zhenjiang, Jiangsu 212001, China
[5]Department of Radiology, Affiliated Hospital of Jiangsu University, Zhenjiang 212001, China
[6]Central Laboratory of the Fourth Affiliated Hospital of Jiangsu University, Zhenjiang, Jiangsu 212001, China
[7]Reproductive Center, The Fourth Affiliated Hospital of Jiangsu University, Zhenjiang, Jiangsu 212001, China

Received: 29 October 2024 / Accepted: 17 February 2025
Published online: 24 February 2025

References

1. Snyder HM, Corriveau RA, Craft S, et al. Vascular contributions to cognitive impairment and dementia including Alzheimer's disease. Alzheimers Dement. 2015;11(6):710–7.
2. You TY, Dong Q, Cui M. Emerging links between cerebral blood flow regulation and cognitive decline: A role for brain microvascular pericytes. Aging Dis. 2023;14(4):1276–91.
3. Li H, Guo Q, Inoue T, et al. Vascular and parenchymal amyloid pathology in an alzheimer disease knock-in mouse model: interplay with cerebral blood flow. Mol Neurodegener. 2014;9:28.
4. Ma C, Hong F, Yang S. Amyloidosis in Alzheimer's disease: pathogeny, etiology, and related therapeutic directions. Molecules. 2022;27(4):1210.
5. Tarasoff-Conway JM, Carare RO, Osorio RS, et al. Clearance systems in the brain-implications for alzheimer disease. Nat Rev Neurol. 2015;11(8):457–70.
6. Malpas CB, Saling MM, Velakoulis D, Desmond P, O'Brien TJ. Alzheimer's disease neuroimaging I. Tau and Amyloid-beta cerebrospinal fluid biomarkers have differential relationships with cognition in mild cognitive impairment. J Alzheimers Dis. 2015;47(4):965–75.
7. Uddin MS, Lim LW. Glial cells in Alzheimer's disease: from neuropathological changes to therapeutic implications. Ageing Res Rev. 2022;78:101622.
8. Hampel H, Hardy J, Blennow K, et al. The Amyloid-beta pathway in Alzheimer's disease. Mol Psychiatry. 2021;26(10):5481–503.
9. Sun X, Chen WD, Wang YD. beta-Amyloid: the key peptide in the pathogenesis of Alzheimer's disease. Front Pharmacol. 2015;6:221.
10. Wang Y, van Gelderen P, de Zwart JA, et al. Cerebrovascular activity is a major factor in the cerebrospinal fluid flow dynamics. Neuroimage. 2022;258:119362.
11. Wong SM, Jansen JFA, Zhang CE, et al. Blood-brain barrier impairment and hypoperfusion are linked in cerebral small vessel disease. Neurology. 2019;92(15):e1669–77.
12. Hong H, Hong L, Luo X, et al. The relationship between amyloid pathology, cerebral small vessel disease, glymphatic dysfunction, and cognition: a study based on Alzheimer's disease continuum participants. Alzheimers Res Ther. 2024;16(1):43.
13. Villain N, Chetelat G, Grassiot B, et al. Regional dynamics of amyloid-beta deposition in healthy elderly, mild cognitive impairment and Alzheimer's disease: a Voxelwise PiB-PET longitudinal study. Brain. 2012;135(Pt 7):2126–39.
14. Fazlollahi A, Calamante F, Liang X, et al. Increased cerebral blood flow with increased amyloid burden in the preclinical phase of Alzheimer's disease. J Magn Reson Imaging. 2020;51(2):505–13.
15. Kim GH, Kim BR, Yoon HJ, Jeong JH. Elevated cerebral blood flow proxy with increased beta-amyloid burden in Alzheimer's disease preclinical phase evaluated by dual-phase (18)F-florbetaben positron emission tomography. Sci Rep. 2024;14(1):18480.
16. Jaroudi W, Garami J, Garrido S, Hornberger M, Keri S, Moustafa AA. Factors underlying cognitive decline in old age and Alzheimer's disease: the role of the hippocampus. Rev Neurosci. 2017;28(7):705–14.
17. Bettio LEB, Rajendran L, Gil-Mohapel J. The effects of aging in the hippocampus and cognitive decline. Neurosci Biobehav Rev. 2017;79:66–86.
18. Meier SR, Sehlin D, Roshanbin S, et al. (11)C-PiB and (124)I-Antibody PET provide differing estimates of brain Amyloid-beta after therapeutic intervention. J Nucl Med. 2022;63(2):302–9.
19. Ismail R, Parbo P, Hansen KV, et al. Abnormal amyloid load in mild cognitive impairment: the effect of reducing the PiB-PET threshold. J Neuroimaging. 2019;29(4):499–505.

20. Perosa V, Priester A, Ziegler G, et al. Hippocampal vascular reserve associated with cognitive performance and hippocampal volume. Brain. 2020;143(2):622–34.
21. Spallazzi M, Dobisch L, Becke A, et al. Hippocampal vascularization patterns: A high-resolution 7 Tesla time-of-flight magnetic resonance angiography study. Neuroimage Clin. 2019;21:101609.
22. Isolan GR, Stefani MA, Schneider FL, et al. Hippocampal vascularization: proposal for a new classification. Surg Neurol Int. 2020;11:378.
23. Elahi FM, Wang MM, Meschia JF. Cerebral small vessel Disease-Related dementia: more questions than answers. Stroke. 2023;54(3):648–60.
24. Pinter D, Enzinger C, Fazekas F. Cerebral small vessel disease, cognitive reserve and cognitive dysfunction. J Neurol. 2015;262(11):2411–9.
25. Xhima K, Ottoy J, Gibson E, et al. Distinct Spatial contributions of amyloid pathology and cerebral small vessel disease to hippocampal morphology. Alzheimers Dement. 2024;20(5):3687–95.
26. Petersen RC, Smith GE, Waring SC, Ivnik RJ, Tangalos EG, Kokmen E. Mild cognitive impairment: clinical characterization and outcome. Arch Neurol. 1999;56(3):303–8.
27. Albert MS, DeKosky ST, Dickson D, et al. The diagnosis of mild cognitive impairment due to Alzheimer's disease: recommendations from the National Institute on Aging-Alzheimer's association workgroups on diagnostic guidelines for Alzheimer's disease. Alzheimers Dement. 2011;7(3):270–9.
28. McKhann G, Drachman D, Folstein M, Katzman R, Price D, Stadlan EM. Clinical diagnosis of Alzheimer's disease: report of the NINCDS-ADRDA work group under the auspices of department of health and human services task force on Alzheimer's disease. Neurology. 1984;34(7):939–44.
29. Chen X, Wang J, Shan Y, et al. Cerebral small vessel disease: neuroimaging markers and clinical implication. J Neurol. 2019;266(10):2347–62.
30. Li Y, Kalpouzos G, Laukka EJ, et al. Progression of neuroimaging markers of cerebral small vessel disease in older adults: A 6-year follow-up study. Neurobiol Aging. 2022;112:204–11.
31. Fazekas F, Chawluk JB, Alavi A, Hurtig HI, Zimmerman RA. MR signal abnormalities at 1.5 T in Alzheimer's dementia and normal aging. AJR Am J Roentgenol. 1987;149(2):351–6.
32. Staals J, Booth T, Morris Z, et al. Total MRI load of cerebral small vessel disease and cognitive ability in older people. Neurobiol Aging. 2015;36(10):2806–11.
33. Fan Y, Shen M, Huo Y, et al. Total cerebral small vessel disease burden on MRI correlates with medial Temporal lobe atrophy and cognitive performance in patients of a memory clinic. Front Aging Neurosci. 2021;13:698035.
34. Patenaude B, Smith SM, Kennedy DN, Jenkinson M. A bayesian model of shape and appearance for subcortical brain segmentation. NeuroImage. 2011;56(3):907–22.
35. Avants BB, Tustison NJ, Song G, Cook PA, Klein A, Gee JC. A reproducible evaluation of ants similarity metric performance in brain image registration. NeuroImage. 2011;54(3):2033–44.
36. Alsop DC, Detre JA, Golay X, et al. Recommended implementation of arterial spin-labeled perfusion MRI for clinical applications: A consensus of the ISMRM perfusion study group and the European consortium for ASL in dementia. Magn Reson Med. 2015;73(1):102–16.
37. Araque Caballero MA, Suarez-Calvet M, Duering M, et al. White matter diffusion alterations precede symptom onset in autosomal dominant Alzheimer's disease. Brain. 2018;141(10):3065–80.
38. Grimm O, Pohlack S, Cacciaglia R, et al. Amygdalar and hippocampal volume: A comparison between manual segmentation, freesurfer and VBM. J Neurosci Methods. 2015;253:254–61.
39. Zeydan B, Schwarz CG, Lowe VJ, et al. Investigation of white matter PiB uptake as a marker of white matter integrity. Ann Clin Transl Neurol. 2019;6(4):678–88.
40. Lee MJ, Seo SW, Na DL, et al. Synergistic effects of ischemia and beta-amyloid burden on cognitive decline in patients with subcortical vascular mild cognitive impairment. JAMA Psychiatry. 2014;71(4):412–22.
41. Fan LY, Tzen KY, Chen YF, et al. The relation between brain amyloid deposition, cortical atrophy, and plasma biomarkers in amnesic mild cognitive impairment and Alzheimer's disease. Front Aging Neurosci. 2018;10:175.
42. Lopez OL, Becker JT, Chang YF, et al. Incidence of mild cognitive impairment in the Pittsburgh cardiovascular health study-Cognition study. Neurology. 2012;79(15):1599–606.
43. Bessi V, Mazzeo S, Padiglioni S, et al. From subjective cognitive decline to Alzheimer's disease: the predictive role of neuropsychological assessment, personality traits, and cognitive reserve. A 7-Year Follow-Up study. J Alzheimers Dis. 2018;63(4):1523–35.
44. Xu Z, Zhang D, Sit RWS, et al. Incidence of and risk factors for mild cognitive impairment in Chinese older adults with Multimorbidity in Hong Kong. Sci Rep. 2020;10(1):4137.
45. Johnson AC. Hippocampal vascular supply and its role in vascular cognitive impairment. Stroke. 2023;54(3):673–85.
46. Thomas KR, Osuna JR, Weigand AJ, et al. Regional hyperperfusion in older adults with objectively-defined subtle cognitive decline. J Cereb Blood Flow Metab. 2021;41(5):1001–12.
47. Zeisel A, Munoz-Manchado AB, Codeluppi S, et al. Brain structure. Cell types in the mouse cortex and hippocampus revealed by single-cell RNA-seq. Science. 2015;347(6226):1138–42.
48. Lana D, Ugolini F, Giovannini MG. Space-Dependent Glia-Neuron interplay in the Hippocampus of Transgenic models of beta-Amyloid deposition. Int J Mol Sci. 2020;21(24):9441.
49. Mufson EJ, Mahady L, Waters D, et al. Hippocampal plasticity during the progression of Alzheimer's disease. Neuroscience. 2015;309:51–67.
50. Tahami Monfared AA, Byrnes MJ, White LA, Zhang Q. Alzheimer's disease: epidemiology and clinical progression. Neurol Ther. 2022;11(2):553–69.
51. Malikova H, Holesta M. Gadolinium contrast agents - are they really safe? J Vasc Access. 2017;18(Suppl 2):1–7.
52. Lee D, Le TT, Im GH, Kim SG. Whole-brain perfusion mapping in mice by dynamic BOLD MRI with transient hypoxia. J Cereb Blood Flow Metab. 2022;42(12):2270–86.
53. MacDonald ME, Berman AJL, Mazerolle EL, Williams RJ, Pike GB. Modeling hyperoxia-induced BOLD signal dynamics to estimate cerebral blood flow, volume and mean transit time. NeuroImage. 2018;178:461–74.
54. Han PK, Choi SH, Park SH. Investigation of control scans in pseudo-continuous arterial spin labeling (pCASL): strategies for improving sensitivity and reliability of pCASL. Magn Reson Med. 2017;78(3):917–29.
55. Dolui S, Vidorreta M, Wang Z, et al. Comparison of PASL, PCASL, and background-suppressed 3D PCASL in mild cognitive impairment. Hum Brain Mapp. 2017;38(10):5260–73.
56. Peng SL, Chu LWL, Su FY. Cerebral hemodynamic response to caffeine: effect of dietary caffeine consumption. NMR Biomed. 2022;35(8):e4727.
57. Leithner C, Royl G. The oxygen paradox of neurovascular coupling. J Cereb Blood Flow Metab. 2014;34(1):19–29.
58. Negri S, Faris P, Pellavio G, et al. Group 1 metabotropic glutamate receptors trigger glutamate-induced intracellular Ca(2+) signals and nitric oxide release in human brain microvascular endothelial cells. Cell Mol Life Sci. 2020;77(11):2235–53.

Publisher's note